CELL BIOLOGY

The local microenvironment limits the regenerative potential of the mouse neonatal heart

Mario Notari,[1]* Antoni Ventura-Rubio,[1] Sylvia J. Bedford-Guaus,[1,2] Ignasi Jorba,[3,4,5] Lola Mulero,[1] Daniel Navajas,[3,4,5] Mercè Martí,[1,2] Ángel Raya[1,2,6]*

Neonatal mice have been shown to regenerate their hearts during a transient window of time of approximately 1 week after birth. However, experimental evidence for this phenomenon is not undisputed, because several laboratories have been unable to detect neonatal heart regeneration. We first confirmed that 1-day-old neonatal mice are indeed able to mount a robust regenerative response after heart amputation. We then found that this regenerative ability sharply declines within 48 hours, with hearts of 2-day-old mice responding to amputation with fibrosis, rather than regeneration. By comparing the global transcriptomes of 1- and 2-day-old mouse hearts, we found that most differentially expressed transcripts encode extracellular matrix components and structural constituents of the cytoskeleton. These results suggest that the stiffness of the local microenvironment, rather than cardiac cell-autonomous mechanisms, crucially determines the ability or inability of the heart to regenerate. Testing this hypothesis by pharmacologically decreasing the stiffness of the extracellular matrix in 3-day-old mice, we found that decreased matrix stiffness rescued the ability of mice to regenerate heart tissue after apical resection. Together, our results identify an unexpectedly restricted time window of regenerative competence in the mouse neonatal heart and open new avenues for promoting cardiac regeneration by local modification of the extracellular matrix stiffness.

INTRODUCTION

Cardiovascular diseases are the leading cause of death in the developed world (*1*), yet identifying a cure remains a major unmet medical goal. Although recent investigations have shown that adult human cardiomyocytes (CMs) can be replaced at a low but detectable rate (*2*), it is well documented that large injuries to the adult heart culminate in replacement of lost CMs with a collagen-rich scar (*3*). This response results in a progressive deterioration of the heart contractile capacity, ultimately leading to end-stage heart failure, which bears a poor prognosis (*3*). Given the lack of therapeutic approaches to reverse the loss of functional myocardium, the development of efficient and safe regenerative procedures is an urgent need in the field of modern cardiovascular research.

Regeneration is a complex biological process by which animals rebuild the shape, structure, and function of body parts lost after injury or experimental amputation. In this context, adult zebrafish can extensively restore CMs lost after surgical removal of a large portion of the myocardium within 60 days from the delivery of the injury (*4*, *5*). In this model, "de novo" tissue formation is accomplished through a series of events that involve dedifferentiation of resident CMs and an increased proliferation index (*6*–*8*). In 2011, Porrello and colleagues (*9*) observed similar regenerative responses in the neonatal (1-day-old) mouse heart after resection of a small portion of the left ventricular apex. After the original report, several other laboratories also reported complete or nearly complete regeneration after partial resection of the left ventricular apex in 1-day-old mice (*10*–*17*). This ability to regenerate their hearts was lost in 7-day-old mice, in which amputation of the ventricular apex was associated with scarring of myocardial tissue and hence a complete lack of regeneration (*9*). Mouse CMs undergo a final round of DNA synthesis without cytokinesis between postnatal days 5 and 7, with most CMs permanently withdrawing from the cell cycle (*18*, *19*). Together, these findings led to the assumption that CMs of newborn mice maintained their proliferative capability and hence the competence to regenerate lost myocardial tissue during the first 7 days of life (*9*, *20*), although this assumed ability was never directly investigated.

Nonetheless, there have also been some discrepancies (*21*–*23*) as to the regenerative ability of the neonatal mammalian heart since the original study of Porrello *et al.* (*9*). For instance, Konfino and colleagues (*23*) reported that heart regeneration in postnatal day 1 newborn mice, after myocardial infarction in a model of left anterior descending artery ligation, was incomplete and was associated with the presence of collagen-rich deposits. However, later independent studies using the same cardiac injury model reported complete scar-free cardiac regeneration (*24*). More recently, Andersen and co-workers (*21*) found no evidence of regeneration after performing an extensive study with long-term follow-up involving apical resection of the heart ventricle in hundreds of neonatal P1 mice from inbred and outbred strains. Other work independently highlighted limitations in the degree of neonatal mouse heart regeneration depending on the type and extent of the injury (*22*).

The molecular determinants of postnatal CM cell cycle withdrawal are only partially understood. Several factors have been proposed to promote CM cell cycle exit, including the transition from the hypoxic intrauterine environment to more aerobic postnatal conditions (*25*), up-regulation of specific classes of microRNAs (*20*, *26*), and the down- or up-regulation of cell cycle regulators (*27*) and growth factors (*28*). Further research is needed to clarify the extent and ability of postnatal CMs to proliferate in response to heart injury, as well as to delineate the mechanisms underlying myocardial regeneration. Here, we investigated the regenerative potential of the neonatal mouse heart by performing amputation of the ventricular apex in mice at postnatal days 1, 2, 3, 4, and 9 (P1, P2, P3, P4, and P9, respectively). Our results confirm previous findings that P1 neonatal mice display a robust cardiac regenerative capacity in response to apex resection. Unexpectedly, heart amputation in P2 animals induced an extensive fibrotic response and subsequent scarring, similar to that observed in P3, P4, and P9 mice. Next, we

[1]Center of Regenerative Medicine in Barcelona (CMRB), Hospital Duran i Reynals, 3rd Floor, Av. Gran Via 199-203, 08098 Hospitalet de Llobregat, Barcelona, Spain. [2]Center for Networked Biomedical Research on Bioengineering, Biomaterials and Nanomedicine (CIBER-BBN), Madrid, Spain. [3]Institute for Bioengineering of Catalonia, 08028 Barcelona, Spain. [4]School of Medicine and Health Sciences, University of Barcelona, Barcelona, Spain. [5]Center for Networked Biomedical Research on Respiratory Diseases (CIBERES), Madrid, Spain. [6]Institució Catalana de Recerca i Estudis Avançats, Barcelona, Spain.
*Corresponding author. Email: araya@cmrb.eu (Á.R.); mnotari@cmrb.eu (M.N.)

investigated the global transcriptome profiles in search of molecular cues that could be responsible for the sharp decline in regenerative potential between P1 and P2 mouse hearts. Differentially expressed transcripts overrepresented gene categories involved in extracellular matrix (ECM) composition. Then, we analyzed the mechanical properties of the heart ECM by atomic force microscopy (AFM) and found that P2 hearts are significantly stiffer than P1. Finally, by decreasing the stiffness of the local microenvironment with a pharmacological inhibitor of the cross-linker enzyme lysyl oxidase (LOX), we were able to rescue the heart regenerative competence of P3 mice. In summary, our combined results identify a surprisingly narrow postnatal time window during which the mouse heart retains the ability to regenerate after injury, and suggest that changes in ECM stiffness and composition are novel and important mechanisms to limit the ability of the mammalian heart to regenerate.

RESULTS

Cardiac regeneration following apical resection in P1 mice

To determine whether apical resection of a small portion of the left ventricle was associated with myocardial regeneration in mammals, we first adapted to our laboratory the technique described by Porrello and colleagues in 2011 (*9*) and detailed by the Sadek group in 2014 (*29*). Our technique differed only in that the fixation step of the ventricular heart section to be amputated was performed using a microsurgery needle rather than blunt forceps (see Materials and Methods), a modification that facilitated accurate control of the amount of tissue resected among individual mice and avoided the issue of surgically retracting the heart (fig. S1A) (*22*).

Next, we investigated whether, in our hands, left ventricular apex amputation in P1 mice was followed by robust tissue regeneration, as previously reported (*9*). P1 mice displayed close to 80% survival following apical resection, a survival rate moderately higher than that reported in the original study (Fig. 1A). In response to the surgical amputation procedure, the hearts of P1 mice ($n = 46$) underwent a marked regenerative process. Stereomicroscopic investigation at 21 days post-amputation (dpa) revealed that apically resected hearts displayed a size and shape comparable to those of hearts from sham-operated siblings, suggesting a hyperplastic rather than hypertrophic response to resection (Fig. 1B). Given that the size of resected tissue had been used as an argument to explain the disparate results obtained among different laboratories with regard to the regenerative ability of the P1 mouse heart (*22*), we measured the resected area in a subset of amputated fragments from P1 hearts using ImageJ software. From eight different measurements, the relative area of resected tissue was comparable among subjects (fig. S1B). At 3 dpa, the hearts of P1 mice exhibited a conspicuous injury, with the presence of disorganized myocardial fibers and sign of acute inflammation (Fig. 1C, white arrowheads). Between 7 and 21 dpa, granulation tissue was gradually replaced by myocardial tissue (Fig. 1C, black arrowheads). To evaluate the remodeling process throughout the injury site of the ventricular apex, we also evaluated six trichrome-stained sections that comprised the entire injury area (as explained in Materials and Methods). We noticed the presence of blue collagen-rich deposits in only two of the six regions spanning the injury site (fig. S1C). Quantification analysis of consecutive trichrome-stained heart sections confirmed a near-complete regeneration of the P1 heart (Fig. 1C). Finally, examination of troponin-I immunolabeled heart sections at 7 and 21 dpa revealed that the area bordering the resection plane contained CMs with dividing nuclei and intercellular spaces, consistent with an infiltration of newly generated CMs (Fig. 1D). Quantitative real-time polymerase chain reaction (qRT-PCR) demonstrated an extremely low expression level of atrial natriuretic peptide (*Nppa*) (fig. S1D) and almost undetectable expression of brain natriuretic peptide (*Nppb*), two important biomarkers with an established role in heart failure (*30*), in P1 amputated organs as compared with sham siblings at 21 dpa. These results suggest the absence of a maladaptive remodeling process of the myocardial tissue and the mounting of a tissue regenerative response.

One fundamental hallmark of myocardial regeneration is the cell cycle reentry of spared CMs (*18*, *31*). To determine whether our in vivo amputation model stimulated cell cycle activity of resident CMs in P1 hearts, animals were pulsed with 5-bromo-2′-deoxyuridine (BrdU) following the apical resection procedure (fig. S1E). Nuclei cell division was assessed by BrdU and troponin-I co-immunostaining, with quantification of the number of proliferating CMs [4′,6-diamidino-2-phenylindole (DAPI)/Tnni3$^+$/BrdU$^+$] at 3, 7, and 21 dpa (fig. S1F). Statistically significant ($P < 0.005$) higher numbers of proliferating CMs were found in apically resected P1 hearts compared with sham hearts at 3, 7, and 21 dpa, both at the site of resection and at a distance from it (Fig. 1E). These data demonstrated that the mouse P1 heart is capable of mounting a robust myocardial regeneration response by enhancing the basal turnover rate of resident CMs.

Fibrotic response after heart amputation in P2 mice

We next subjected P2 mice ($n = 95$) to our apical resection technique. About 75% of P2 neonates survived the surgical procedure, with maternal cannibalization only slightly affecting the survival rate by further lowering this to 66.4% (Fig. 2A). Unexpectedly, stereomicroscopic examination of the apically resected P2 hearts at 21 dpa demonstrated the presence of white fibrotic patches in the external ventricular wall (Fig. 2B, black arrowheads). Over the time course of the study, amputated P2 hearts consistently weighed less than those from sham siblings, suggesting a lack of myocardial tissue regeneration (Fig. 2C). Histological analysis of serial sections at 21 dpa revealed evident signs of cardiac remodeling with increased interstitial fibrosis, which was confirmed by quantification analysis of the scar area in serial trichrome-stained heart sections (Fig. 2D). To exclude the possibility of a delayed regeneration process in P2 mice, we extended the examination period of tissue sections to 35 dpa. However, fibrotic deposits were still present at that time (fig. S2A). To assess whether CMs were present in the repaired tissue region of P2 hearts, we performed immunofluorescence staining for cardiac troponin-I. The cardiac protein was not detected at any of the stages of the myocardial repair process within the remodeled tissue, despite the presence of cell infiltration in the area as demonstrated by DAPI staining (Fig. 2E), and was more evident in higher-magnification images of these sections at 21 dpa (fig. 2B). These data indicate that hearts of 2-day-old mice responded to amputation with fibrosis rather than regeneration. No statistical differences in the expression levels of *Nppa* and *Nppb* were observed between amputated and sham-operated hearts at 21 dpa (fig. S2C). On the other hand, the expression level of *Col3a1*, important component of fibrous connective tissue (*32*), in amputated hearts was higher at 21 dpa when compared to sham siblings (fig. S2D), suggesting an active deposition of newly synthesized ECM. Next, we investigated CM proliferation in BrdU pulse-chase experiments on P2 mice (fig. S2E). Hearts were obtained at 3, 7, and 14 dpa to assess CM proliferation by colocalization of BrdU and a cardiac-specific antibody against myosin heavy chain (MF-20) (fig. S2F). No statistically significant differences were detected on the numbers of BrdU$^+$ CMs in amputated relative to sham-operated hearts at 3, 7, or 14 days after resection. Moreover,

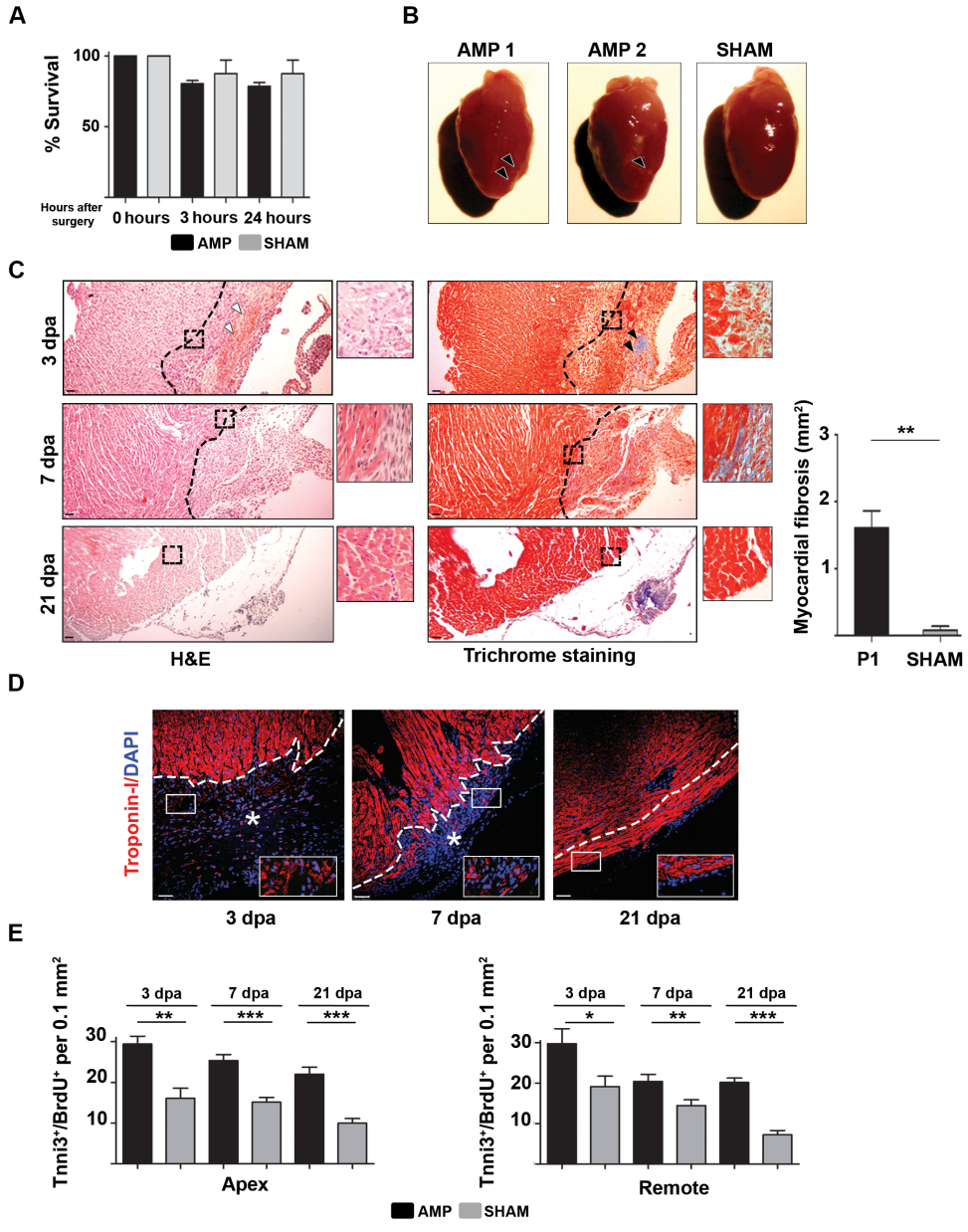

Fig. 1. Regeneration of the heart in P1 mice following surgical resection of a small portion of the left ventricular apex. (**A**) Survival of P1 mice that underwent apical amputation (AMP; $n = 46$) or not (SHAM; $n = 31$). Animal survival was determined immediately (0 h), after 3 hours (3 h), and the day after surgery (24 h). Means ± SEM. (**B**) Stereomicroscopic pictures of AMP and SHAM hearts at 21 dpa showed similar heart morphology with only minimal fibrosis evident in the external ventricular wall (black arrowheads). (**C**) Representative hematoxylin and eosin (H&E)– and trichrome-stained sections of the apex of resected hearts at various stages of regeneration. Cardiac tissue loss is evident at 3 and 7 dpa by the misalignment of tissue fibers (H&E inset) and by the presence of blue staining evidencing collagen deposition (trichrome stain inset). Notably, at 21 dpa, fiber misalignment and blue collagen deposits were evident only in tissue outside the ventricular wall. White arrowheads indicate acute inflammation, and black arrowheads indicate granulation tissue, whereas the dashed line marks the lesion border. Scale bars, 50 μm. Right: Quantification analysis of the scar area in P1 AMP versus SHAM at 21 dpa. (**D**) Immunofluorescence staining for troponin-I and DAPI at 3, 7, and 21 dpa. An asterisk indicates the healing area, whereas the dashed line marks the lesion border. Scale bars, 25 μm. (**E**) Number of proliferating CMs ($DAPI^+/Tnni3^+/BrdU^+$ cells) per 0.1 mm^2 counted in paraffin-embedded SHAM ($n = 3$) and AMP ($n = 5$) heart sections from BrdU multiple pulse-chase experiments at the indicated dpa. Data are means ± SEM. Only fields completely filled with cells were included in the analysis. *$P < 0.05$; **$P < 0.01$; ***$P < 0.001$.

proliferating CMs in areas away from the injury were also similar in number in both experimental groups (Fig. 2F).

Inconsistent results between laboratories with regard to the regenerative ability of the postnatal mouse heart had been partially justified on the basis of the relative size of resected tissue (*22*, *23*). Therefore, we compared the heart–to–body weight ratio between P2 amputated ($n = 6$) and sham-operated ($n = 4$) mice 3 hours after surgery to calculate the relative percentage of amputated myocardial tissue in these experiments. Our calculations showed a consistent reduction of ~13% of weight in amputated hearts relative to that of sham-operated hearts (fig. S2G).

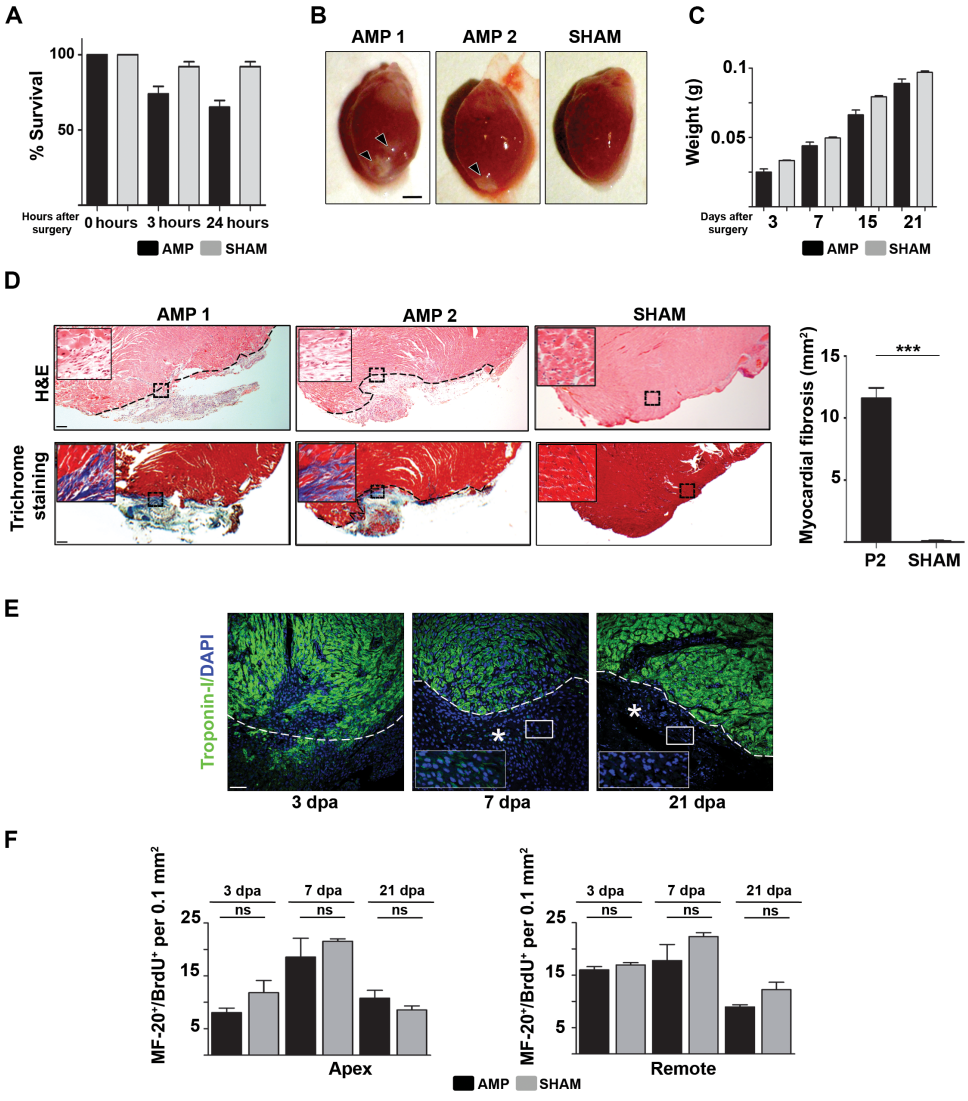

Fig. 2. Scar and new myocardial tissue assessment following surgical amputation of the left ventricular apex in P2 mice revealed a lack of myocardial regeneration. (**A**) Survival of P2 mice that underwent amputation (AMP; $n = 91$) or not (SHAM; $n = 51$) of a small portion of the left ventricular apex. Animal survival was determined immediately (0 h), after 3 hours (3 h), and the day after surgery (24 h). Data are means ± SEM. (**B**) Stereomicroscopic pictures of AMP and SHAM hearts at 21 dpa demonstrated the presence of extensive white patches on the external ventricular wall 21 days following surgery (black arrowheads). Scale bar, 1 mm. (**C**) Heart weight of P2 AMP ($n = 3$) and SHAM ($n = 3$) mice was determined at different time points following surgery. (**D**) Representative H&E- and trichrome-stained sections of P2 hearts at 21 dpa. Cardiac tissue loss is evident by the misalignment of tissue fibers (H&E inset) and by the presence of intense blue staining (trichrome inset). Dashed line marks the lesion border. Scale bar, 200 μm. Right: Quantification analysis of the scar area in P2 AMP versus SHAM at 21 dpa. ***$P < 0.001$. (**E**) Paraffin-embedded resected P2 hearts were sectioned and immunostained for troponin-I and DAPI. Representative images at various time points during the post-AMP process demonstrate an absence of newly formed myocardial tissue. An asterisk indicates the healing area, whereas the dashed line marks the lesion border. Scale bar, 25 μm. (**F**) Number of proliferating CMs ($DAPI^+/MF\text{-}20^+/BrdU^+$ cells) per 0.1 mm^2 counted in paraffin-embedded SHAM and AMP heart sections from BrdU multiple pulse-chase experiments at the indicated dpa. Data are means ± SEM; $n = 3$. Only fields completely filled with cells were included in the analysis. ns, not significant.

Hence, our surgical technique consistently removed less than 15% of the heart tissue, a value that was previously associated with full regeneration, at least in P1 mice (*22*). Moreover, quantification of the resected area using imaging software further supported the consistency of our technique and reproducibility of our data (fig. S2H). Together, these data show that amputation of the left ventricular apex in P2 neonatal mice induced a healing response characterized by massive fibrotic deposition, which resulted in substantial scarring of the heart, in sharp contrast with the regenerative response observed in P1 neonatal mice.

Absence of heart regeneration in P3 and older mice

Amputation of the left ventricular apex in P3 ($n = 18$) and P4 ($n = 5$) neonatal mice resulted in fibrotic responses similar to those observed in P2 animals. In both P3 and P4 groups, only about 60% of neonates survived the surgical procedure (fig. S3A), despite the fact that the relative area of resected myocardial tissue was comparable with that of experiments performed in P2 mice (fig. S3B). When analyzed at 21 dpa, visible white patches on the external ventricular wall, corresponding to fibrotic deposits in both groups, were observed (fig. S3C, black arrowheads). At the

histological level, all resected hearts examined showed extensive remodeling of damaged myocardium with the presence of scar tissue and collagen deposition at 21 dpa (fig. S3C, bottom), suggesting an ongoing fibrotic response similar to the one seen in P2 hearts.

We also performed surgical amputation of the ventricular apex in P9 mice (n = 38). Survival of resected P9 mice was lower than 50%, indicating that the surgical procedure was not well tolerated at this age (fig. S4A). The surviving mice responded with evident fibrotic deposits (fig. S4B, black arrowheads). At the histological level, all resected hearts analyzed showed a considerable remodeling of the architecture of the myocardial tissue with the presence of scar tissue and collagen deposition at 21 and 35 dpa, as shown by trichrome-stained images of heart sections (fig. S4, C and D). Immunofluorescence staining using an antibody against troponin-I further corroborated the absence of CMs in scar tissue at 21 dpa (fig. S4E). Furthermore, expression levels of *Nppa*, *Nppb*, and *Col3a1* were significantly increased in P9 amputated hearts when compared to sham siblings at 21 dpa (fig. S4F), supporting an ongoing hypertrophic maladaptive response.

Transcriptional profiling of P1 and P2 mouse hearts

To gain insight into the molecular factors responsible for the abrupt decline in heart regeneration competence between P1 and P2 mice, we first compared the transcriptome profile of control, uninjured hearts of 1- and 2-day-old mouse neonates. For this purpose, we performed RNA sequencing (RNA-seq) of nonmanipulated P1 and P2 ventricular tissue (n = 3). As expected, because of the overall similarity of both types of sample, most detected transcripts displayed comparable expression levels in P1 and P2 hearts (~7800 genes). A small but consistent group of transcripts showed differential expression (up- or down-regulation) in P2 versus P1 hearts (192 and 159 gene products, respectively) (Fig. 3A and fig. S5A; see also list of transcripts in Supplementary Dataset). We validated the RNA-seq results by measuring the expression of randomly selected (up- or down-regulated) genes by qRT-PCR analysis (fig. S5B). We also measured the expression levels of specific ECM-related transcripts identified as differentially expressed in our RNA-seq analysis, as well as of *Dag1* (encoding dystroglycan 1) and *Agrin*, two genes recently described to regulate mammalian heart regeneration (*15*, *16*). For this purpose, qRT-PCR analyses were carried out on ventricular tissue RNA from P1 and P2 mice, using specific primers spanning exon-exon junctions of the genes of interest. Increased expression of the ECM-related genes *Mfap5*, *Aspn*, and *Itga6* was found in hearts of P2 compared to P1 neonatal mice, whereas no differences were observed for *Agrin* or *Dag1* (fig. S5C), further validating the results of our RNA-seq analysis.

Enriched gene ontology (GO) term analysis of differentially expressed transcripts between P2 and P1 mouse hearts revealed an overrepresentation of genes related to ECM binding and assembly (Fig. 3B), such as collagens V and VIII (*Col5a3* and *Col8a1*), microfibrillar-associated protein 5 (*Mfap5*), decorin (*Dcn*), metalloproteinase with thrombospondin motifs 5 (*Adamts5*), and thrombospondin-1 (*Thbs1*). In line with this, genes that were also involved in integrin binding processes such as integrin β-6 (*Itgb6*), integrin α-7 (*Itga7*), vitronectin (*Vtn*), and endothelial molecule 1 (*Esm1*) displayed higher expression levels in hearts of P2 mice than in those of P1 mice. GO term analysis further revealed that transcripts for proteins contributing to the structural integrity of the sarcoplasm such as myosin-binding protein C (*Mybpc1* and *Mybpc2*), myosin light chain kinase (*Mylk4*), myomesins 1 and 2 (*Myom1* and *Myom2*), and microtubule-associated protein tau 2 (*Mapt*) also showed a pronounced up-regulation over the course of 24 hours, reflecting increased organization and assembly of the CM cytoskeleton. Conversely, mRNAs down-regulated in P2 hearts compared with P1 belonged to the family of genes that function within the acetyl coenzyme A metabolic pathway. Overall, the GO bioinformatic analysis of the transcriptional changes that occur in the mouse heart between P1 and P2 revealed that the developing mammalian heart rapidly up-regulates ECM components, as well as structural sarcomere genes.

Contrary to our initial expectations, GO term analysis did not reveal differences in the expression of cell cycle regulators such as cyclin, cyclin-dependent kinases (CDKs), and/or CDK inhibitors between P1 and P2 hearts (Fig. 3B). However, this was consistent with the fact that P1 and P2 hearts contained similar percentages of cycling CMs (Fig. 3C). Moreover, we also quantified the number of mono- and binucleated CMs in P1 and P2 operated hearts at 3 and 7 dpa. We observed similar high percentages of mononucleated CMs in both P1 and P2 hearts at 3 dpa (P1, 80.7 ± 0.76%; P2, 77.5 ± 3.21%), as well as similar low percentages of binucleated CMs (P1, 19.2 ± 1.15%; P2, 22.4 ± 3.21%), in line with a previous report (*19*). At 7 dpa, we found an increase in the percentage of binucleated CMs in both P1 and P2 hearts as expected, albeit lower than previously reported (*19*), most likely due to methodological differences in the labeling/scoring techniques, but again, no statistically differences were detected between the two experimental groups (Fig. 3D). Our cumulative results thus far indicate that the loss of regenerative competence that takes place in the mouse P2 heart appears mechanistically unrelated to the postnatal switch in CM cell cycle dynamics. Moreover, our transcriptomic analyses identify major changes in ECM composition occurring concomitantly with the transition from regeneration competence to regeneration incompetence.

Rescue of heart regeneration competence after decreasing ECM stiffness

To ascertain the effect of differentially expressed genes encoding ECM components on the actual ECM composition, we first quantified the levels of structural ECM components in protein extracts from P1 and P2 ventricular myocardial tissue, including collagen II, collagen IV, elastin, and laminin. P2 hearts consistently expressed more ECM proteins than P1 hearts (Fig. 4A). Next, we measured the overall stiffness of the heart ECM in P1 and P2 mice by AFM quantification of decellularized whole heart sections. P2 heart ECM was ~50% stiffer than that of P1 hearts (Fig. 4B). These findings suggest that cross-linking of ECM components is important to regulate stiffness of the heart in vivo.

It has been shown that the expression levels of transcripts encoding the ECM cross-linker enzyme LOX are developmentally regulated and might modulate ECM stiffness in neonatal mouse tissues (*33*). Moreover, pharmacological inhibition of LOX using 3-aminopropionitrile (BAPN) was shown to reduce lung ECM stiffness in newborn mice (*34*). Hence, to determine whether changes in ECM stiffness could influence the regenerative capacity of neonatal mouse hearts in vivo, we inhibited collagen and elastin cross-linking by treating mice with the pharmacological LOX inhibitor BAPN (*22*). For this purpose, BAPN was added to the drinking water of pregnant mice from 5 days post-coitum (dpc) until 3 days post-partum [BAPN is known to be secreted into the breast milk (*34*)]. Newborn mice were then sacrificed at P3, and their hearts were processed for immunofluorescence analysis of major ECM components, including collagens II and IV, fibronectin, and laminin. As expected, BAPN-treated hearts lost the fine network of collagens II and IV but showed normal distribution of laminin and fibronectin (Fig. 4C). ECM stiffness, directly measured by AFM in decellularized slices of control and BAPN-treated P3 hearts, was significantly reduced by ~35% after treatment with the LOX inhibitor (Fig. 4D). Once verified

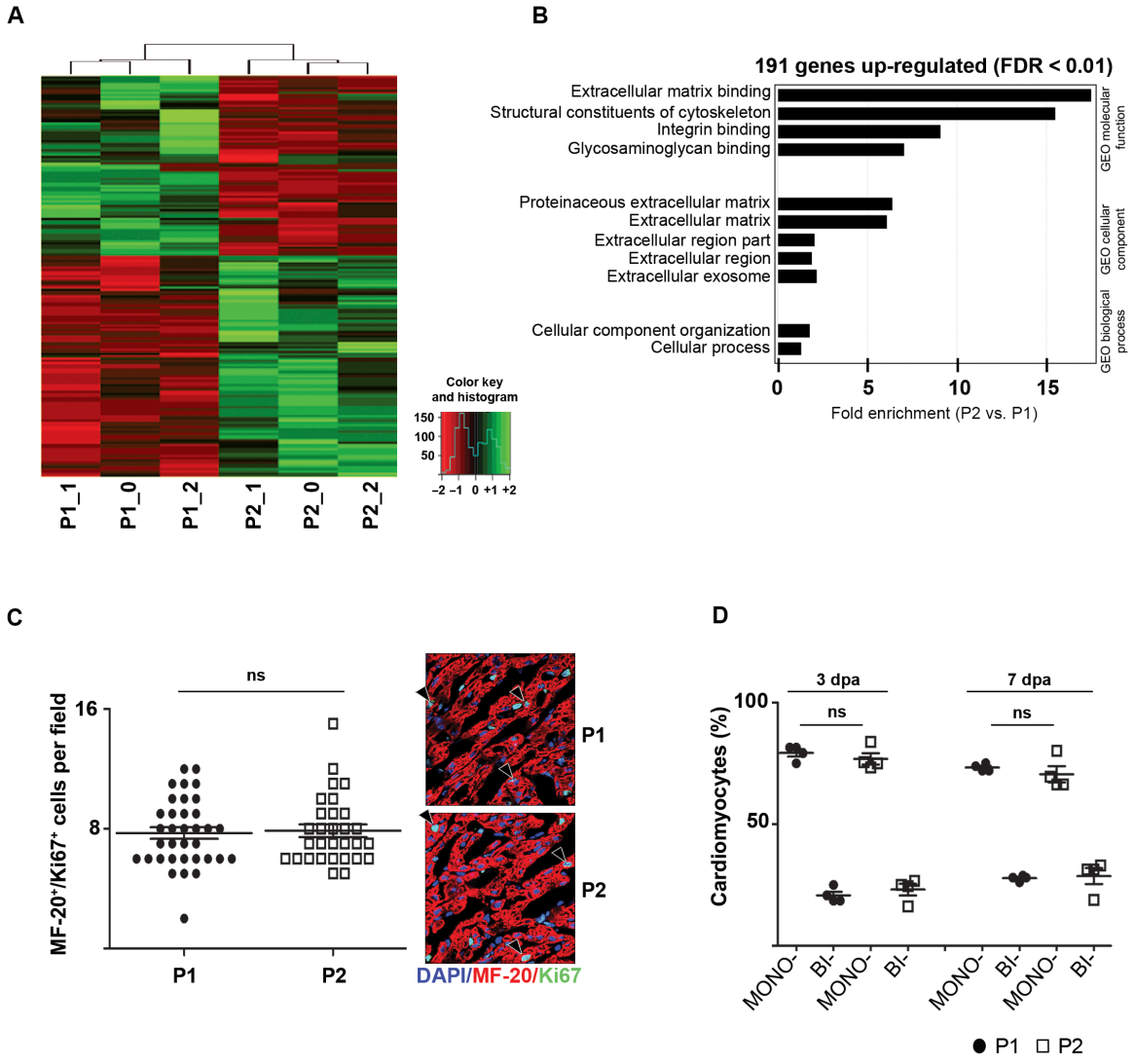

Fig. 3. Differentially expressed genes in the ventricles of hearts from P1 and P2 mice. (**A**) Heat map showing the most differentially expressed (up- or down-regulated) genes in individual hearts from P1 and P2 mice. Shaded color bar represents low (red) to high (green) expression level changes. (**B**) GO analysis of differentially expressed genes between P1 and P2 hearts showing that the most differentially expressed genes belong to structural constituents of myoskeleton and of the ECM. FDR, false discovery rate. (**C**) Left: Quantification of MF-20$^+$/Ki67$^+$ CMs at 1-day-old (P1) or 2-day-old (P2) newborn mice; n = 3. Right: Representative immunofluorescence pictures of P1 and P2 heart sections display positive signal for myosin heavy chain (MF-20) and Ki67. DAPI was used to visualize CM nuclei. Black arrowheads indicate double-positive CMs. (**D**) Quantification analyses (%) of the mononucleated (MONO-) or binucleated (BI-) CMs at different time points during cardiac regeneration carried on hearts of P1 and P2 mice.

that BAPN treatment was effective in reducing heart ECM stiffness, in another series of experiments, we subjected control and BAPN-treated P3 neonatal mice to amputation of the ventricular apex and analyzed whether heart regeneration had occurred at 21 dpa (Fig. 5, A to C). In agreement with our findings that P2 or older mice had lost the ability to regenerate their hearts (see Fig. 2 and figs. S2 to S4), apical amputation in untreated P3 neonatal mice resulted in extensive scarring and failure to regenerate the amputated myocardium after 21 days (Fig. 5, A to D). BAPN treatment prevented to a large extent the fibrotic response to injury in apically resected P3 hearts at 21 days after surgery (Fig. 5, A to D). Quantification of Masson's stained serial transversal sections of amputated hearts of control or BAPN-treated P3 neonatal mice at 21 dpa confirmed that the damaged area was significantly reduced in the BAPN-treated group when compared with the control one (Fig. 5, C and D). We ruled out a direct effect of the BAPN treatment on the CM proliferation rate by directly counting the numbers of MF-20/Ki67 double-positive cells, which showed no differences between control and BAPN-treated P3 neonatal hearts (Fig. 5E). These data indicate that, by decreasing the stiffness of the heart ECM in 3-day-old mice, we rescued their ability to mount a regenerative response after apical resection.

DISCUSSION

We have shown that P1 mice display a robust capacity to regenerate their hearts upon experimental amputation of ~15% of the apex, thus confirming the original findings by Porrello and colleagues (*9*). At this point, the reasons behind the conflicting results obtained by others (*21*, *35*) are not entirely clear. In our studies, given that an inverse

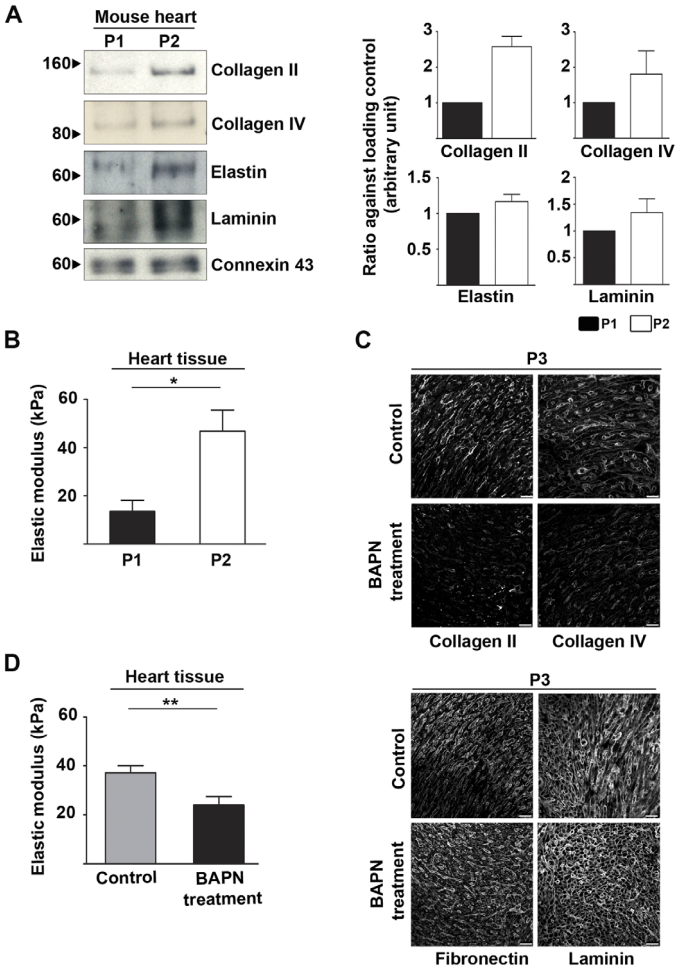

Fig. 4. P1 and P2 hearts show differences in the ECM expression and stiffness; BAPN treatment reduced tissue stiffness in P3 mice. (**A**) Left: Protein levels of ECM components were detected in ventricular heart tissue of P1 and P2 mice by immunoblotting using specific antibodies against collagen II, collagen IV, elastin, and laminin. Junctional connexin 43 protein was used as a loading control. A representative blot from three independent experiments is shown for each panel. Notably, each panel was cropped to better illustrate the difference between P1 and P2. Full-length blots are presented in fig. S6A. Right: Densitometry analysis of three independent Western blot experiments. (**B**) Graph showing the overall stiffness as measured using AFM in decellularized sections of P1 and P2 neonatal mouse hearts; $n = 3$. (**C**) Immunofluorescence showing the distribution of collagens II and IV (top) and fibronectin and laminin (bottom) in heart sections of P3 mice after treatment with BAPN and in control littermates. Scale bars, 50 μm. (**D**) Graph showing the overall stiffness as measured using AFM in decellularized sections of control and BAPN-treated P3 neonatal mouse hearts; $n = 3$. $^{*}P < 0.05$, $^{**}P < 0.01$.

correlation between the extent of regeneration and the size of amputated tissue had been postulated (*22*), our surgical technique was purposely designed to control for the amount of amputated myocardial tissue among experiments and across the different age-dependent heart sizes (figs. S1B, S2H, and S3B). Hence, we limited to less than 15% the proportion of heart tissue amputated, the purported threshold above which complete regeneration may not occur (*22*). We also carefully timed our experiments with the time of parturition, thus ensuring that pups used were exactly of the age reported (±3 hours). Given the striking differences in the regenerative ability between P1 and P2 mice, we speculate that age differences of more than 12 hours at this stage could have a pronounced impact on the results. Therefore, it is plausible that some of the differences reported in the regenerative ability of the heart from newborn mice among studies could be related to actual age differences between pups.

An unexpected finding of our studies is that the hearts of P2 mice, in sharp contrast with those of P1 neonates, do not regenerate in response to experimental amputation. Experimentally convincing evidence as to why or how the neonatal heart regenerates (whereas the adult one does not) is for the most part missing. However, an intellectually satisfying explanation of this fact posited that the heart's regenerative ability was related to the developmental window before CMs became binucleated and withdrew from the cell cycle (*9*, *18*, *25*, *31*). It had been shown that most of the CMs in neonatal mice become postmitotic cells after P5 to P7 (*18*). However, detailed analysis of myocytes isolated from neonatal rat hearts suggested that, after P3, the number of myocytes in the heart remained relatively constant (*36*), suggesting that hyperplastic growth was almost complete at that time. Moreover, a careful analysis of DNA synthesis and binucleation in CMs during murine development showed a marked switch in these processes taking place between days 4 and 7 after birth (*19*). In agreement with those findings, here, we did not detect any differences in cell cycle or binucleation indexes between P1 and P2 hearts. Together, these data provide strong evidence disconnecting the loss of regenerative competence in the mouse neonatal heart from the postnatal switch in CM cell cycle dynamics. That is, if the regenerative potential of the neonatal heart depended on CMs maintaining their ability to proliferate, then it would be expected that neonates could regenerate their hearts until postnatal days 3 to 5, as has been suggested (*9*), but never experimentally addressed. However, our data show that mouse hearts have lost their competence to regenerate as early as P2, that is, long before the hyperplastic-to-hypertrophic transition takes place (*37*). It should be noted that, although our data support the hypothesis that the postnatal switch in CM cell cycle dynamics is not responsible for the loss of heart regenerative competence, our studies do not resolve whether the responsible mechanisms involve the disappearance of neonatal inductive signals for regeneration, the appearance of barriers to regeneration in the adult, or both. Neonatal heart regeneration is a complex phenomenon in which the response to injury is superimposed on the background of normal development, making it hard to tease both types of mechanisms apart. We trust that narrowing down the window of time when the neonatal heart is competent for regeneration will facilitate future research into this topic.

Our finding that P1 and P2 mouse hearts, in spite of their close similarities in size, developmental state, and overall cell cycle profile, radically diverge in their regenerative potential provides an immediate experimental opportunity for addressing the molecular bases of mammalian heart regeneration. Comparative transcriptomic analysis of whole P1 and P2 heart ventricles attested to the overall resemblance between these two developmental stages, with more than 95% of detected transcripts being similarly expressed (fig. S5A). However, we did detect a small number of differentially expressed genes. Specifically, 1.9% of all detected transcripts were found to be expressed at significantly higher levels in P1 than P2 hearts, whereas 2.4% of the transcripts showed higher expression in the hearts of P2 mice compared with those of P1 neonates. Although further investigation will be necessary to ascertain the functional relevance of these differentially expressed transcripts in the context of heart regeneration, the results of our first analyses give new insights into this process. Thus, a search for enriched GO categories within this data set did not detect GO annotations related to cell cycle regulation, lending

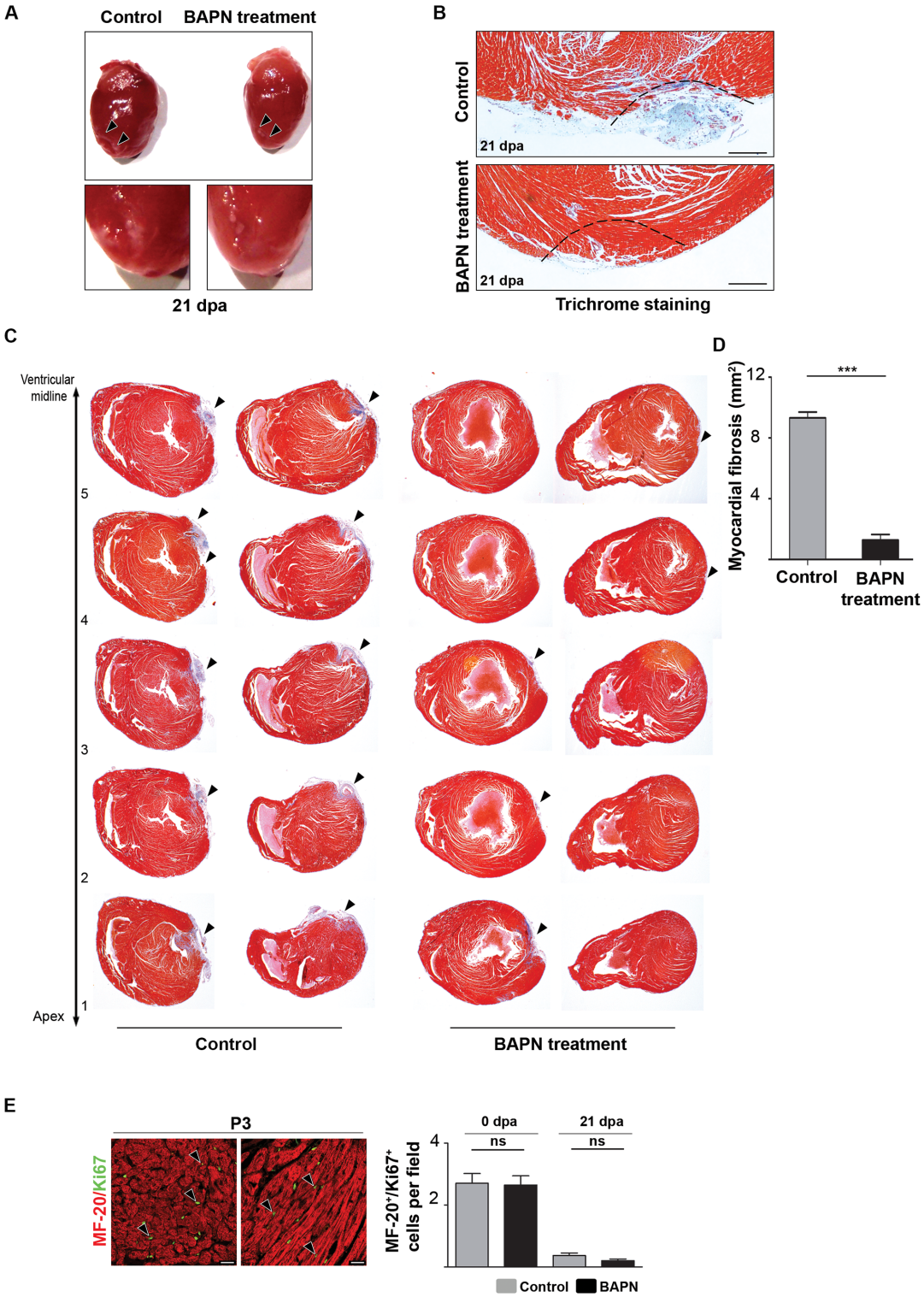

Fig. 5. Decreasing ECM stiffness rescues heart regeneration capacity of P3 mice. (**A**) Stereomicroscopic pictures of control or BAPN-treated P3 neonatal mouse hearts at 21 dpa showed similar heart morphology, but fibrotic patches (black arrowheads) were much more evident in the external ventricular wall of control hearts. (**B**) Representative trichrome-stained sections of control and BAPN-treated P3 neonatal mouse hearts at 21 dpa. Dashed lines mark the amputation plane. Scale bars, 200 μm. (**C**) Serial transverse sections of trichrome-stained hearts of two control and two BAPN-treated neonatal mice at 21 dpa. Collagen deposits are indicated by black arrowheads. (**D**) Quantification analysis of the scar area in control and BAPN-treated P3 neonatal mice at 21 dpa; $n = 3$. (**E**) Left: Representative immunofluorescence images of heart sections showing positive signal for myosin heavy chain (MF-20) and Ki67. DAPI was used to visualize CM nuclei. Black arrowheads indicate double-positive CMs. Scale bars, 25 μm. Right: Quantification of proliferating CMs (MF-20$^+$/Ki67$^+$ cells) in control and BAPN-treated P3 neonatal mouse hearts before (0 dpa) or at 21 dpa. Data are means ± SEM; $n = 3$. ***$P < 0.001$; ns, not significant.

further support to our hypothesis that the regeneration competence of the neonatal mouse heart is not limited by the proliferation ability of CMs. In contrast, we detected significant enrichment of GO categories related to ECM components and integrin binding, as well as structural constituents of the cytoskeleton (Fig. 3B). These findings were further corroborated through protein expression analysis for collagens II and IV, elastin, and laminin—major components of the ECM (Fig. 4A).

It has been shown that the composition and mechanical properties of cardiac ECM greatly vary during the transition from the intrauterine environment to the postnatal life, and this has been mechanistically linked with the appearance of heart disease (*38*). The elastic modulus calculated in samples of developing ventricular tissue in rats showed a clear discontinuity and immediate increase at birth (*39*), supporting our hypothesis that local microenvironment may affect CM behavior and so cardiac regeneration. No major changes have previously been noted to occur between P1 and P2 mouse hearts to our knowledge. Overall, the ECM is considered an important component of the heart maturation process through either direct interaction with cells or modulation via growth factor stimulation (*40*). Recent investigations have demonstrated that the ECM protein Agrin can act as a new inducer of mammalian heart regeneration (*15*) and that the dystrophin glycoprotein complex (DGC), a multicomponent transmembrane complex linking actin cytoskeleton to the ECM, is essential for cardiac regeneration, whereas the DGC component Dag1 inhibits cardiac regeneration (*16*). However, we could not detect differences in the expression levels of *Agrin* or *Dag1* between P1 and P2 neonatal mouse hearts, making it unlikely that these factors mediate the competence to regenerate in this context. Mechanical properties such as stiffness and flexibility constitute a third mechanism that may account for how the ECM controls cell function (*41*, *42*). Hence, rigid matrices facilitate nuclear division (karyokinesis) leading to binucleation, whereas flexible matrices promote CM mitotic rounding and cell division (cytokinesis) (*43*). Along these lines, our results indicate that important changes in ECM stiffness take place in the mouse heart between P1 and P2. However, the mechanisms by which those changes affect neonatal mouse heart regeneration do not appear to involve differences in CM division or binucleation, which we show are comparable in P1 and P2 mouse hearts (Fig. 3, C and D). Nevertheless, the fact that experimental manipulation of the ECM cross-linking to reduce its stiffness partially restores the regenerative competence of P3 mouse hearts provides evidence in favor of a causal link between the two processes. Overall, our results are compatible with a scenario in which the marked changes in heart ECM stiffness that take place in the neonatal mouse between postnatal days 1 and 2 are, at least in part, responsible for the loss of regenerative ability. It is well established that the ECM not only stabilizes and maintains the structure of tissues and organs but also can determine various cellular behaviors such as migration, adhesion, and proliferation. Further research will be needed to dissect the exact mechanisms by which changes in ECM stiffness mediate the loss of regeneration competence in the mouse neonatal heart.

The key to understanding the regenerative potential of the mammalian heart lies within the developmental transitions occurring during the first few days of neonatal life. In this regard, the ability of the immature mammalian heart to regenerate and the subsequent loss of this potential provide an important tool for understanding regeneration competence. Our findings indicate a novel temporal window in which to study the cellular and molecular processes leading to the limited regenerative potential of the adult mammalian heart. Moreover, our data point at the microenvironment and its varying stiffness as a novel mechanism that influences myocardial regeneration competence. Understanding these processes in detail will help to identify regeneration inductive factors and/or development-associated regeneration constrains and generate new targets for therapeutic manipulation.

MATERIALS AND METHODS

Animals

Eight-week-old female and male ICR/CD1 mice were purchased from Charles River Laboratories España S.A. and bred according to routine guidelines. Animals were housed in individually ventilated cages in a 12-hour/12-hour light/dark cycle and fed ad libitum. All animals were handled according to Institutional Animal Care and Use Committee guidelines. All procedures involving animals were approved by and in accordance with the Animal in Science Regulation Unit at the Generalitat de Catalunya (Spain), and the following procedures were approved by the Ethical Review Committee of the Barcelona Biomedical Research Park (PRBB) Animal Committee.

Ventricular apex resection procedure

The left ventricular apex resection procedure used here is diagrammed in fig. S1A. With pups anesthetized by hypothermia, apical resection was performed after lateral thoracotomy at the fourth intercostal space and dissection of the intercostal muscle (fig. S1A). Differences between our procedure and that previously described lie in the fact that we gently lifted the left ventricular apex upward using a needle inserted above the portion to be resected. Then, we excised the portion of myocardial tissue immediately below the needle using micro-ophthalmic scissors (fig. S1A). By inserting the microsurgery needle in the same position for each amputation, we were able to ensure a reproducible procedure with regard to the location and size of resected myocardial tissue (figs. S2A and S3B). This is important because the size of amputated tissue was a potential source of discrepancy that could explain the different results reported by previous groups (*22*). Apical resection surgery was performed on postnatal days 1 (P1), 2 (P2), and 9 (P9). Mating pairs were monitored daily and separated once a plug was detected. Following 19 days, pregnant females were monitored every 12 hours for birthing to allow for accurate aging of newborn pups and timing of the surgical procedure. For surgery, neonates were anesthetized by inducing hypothermia on ice. For amputation, anesthetized neonatal mice were immobilized under a stereomicroscope and subjected to a lateral thoracotomy incision at the fourth intercostal space to expose the heart. A microsurgery needle was used to gently fix in place the apex of the heart. Amputation of a small portion of the ventricular apex was performed in one single cut using angled iridectomy scissors. The thoracic wall incision was then sutured using a continuous pattern with 7-0 silk. Neonates were then removed from the ice bed and placed on a heat pad for recovery. Pups were returned to their dam when spontaneous movement and a red/pink complexion returned. From anesthesia induction to full recovery, the entire procedure took no more than 10 min. Sham-operated mice underwent the same procedures with the exception of heart fixation or resection. Following surgery, animals were checked every 24 hours for 3 days, and any pups not recovering well from surgery or displaying complications were euthanized. The postsurgical survival rate was also recorded.

Heart tissue recovery

Sham-operated and apically resected hearts were harvested at different time points following surgery. For this purpose, mice were euthanized

either by decapitation (<21 days of age) or by cervical dislocation (>21 days of age). Hearts were carefully dissected, avoiding any further damage, washed in phosphate-buffered saline (PBS)/heparin (SAD, 5000 IE/ml), and then processed appropriately for further analysis. To determine the percent of heart amputated in our experiments, a set of each six resected and sham-operated pups were weighed following surgery and before euthanasia. Then, hearts were resected and washed in PBS/heparin (SAD, 5000 IE/ml) to flush out any residual blood from ventricles. Following dissection of any noncardiac annexa and the atria, the ventricles were carefully dried and weighed. Then, for each of the pups, the heart–to–body weight ratio was calculated and then averaged across resected and sham-operated mice, respectively. With sham-operated mice given an arbitrary value of 1, the heart–to–body weight ratio difference between the two groups of mice was used to estimate the average percentage of heart that had been amputated. In addition, for the same set of hearts, the piece of amputated myocardium was photographed under a stereomicroscope, and the area of each piece was calculated in arbitrary units using ImageJ software.

Histological analyses

Mouse hearts at various stages following surgery were dissected as above and processed for histological examination. We noticed that a weak superficial adhesion often formed between the pericardium and pleural surface of the chest wall in animals having undergone apical resection. This was carefully dissected to avoid leaving any heart tissue behind. Mice sacrificed at 21 dpa were previously injected with 20 µl of heparin (50,000 U/ml) to prevent blood clot formation. Dissected hearts were rinsed in warm PBS, blotted on 3MM paper to remove excess fluid, weighed, and then fixed overnight in 2% paraformaldehyde at 4°C. After washing, hearts were embedded whole in paraffin and sectioned. We performed consecutive serial 5-µm-thick sections that spanned throughout the injured area of the heart. Every 10 sections were consecutively placed on a different glass slide for staining and evaluation. Ultimately, each glass slide contained six sections that represented consecutive three-dimensional regions across the injured area 50 µm apart. Therefore, for each staining performed, this permitted a thorough evaluation of any changes spanning the entire region of interest.

Masson's trichrome and H&E staining were performed on deparaffinized heart sections according to the manufacturer's instructions (Sigma-Aldrich). Images were analyzed using ImageJ software, and the extent of scarring was calculated as the area of fibrotic infiltration (blue color in Masson's trichrome staining) across the injured area. For immunofluorescence, sections were deparaffinized and rehydrated before antigen retrieval (DAKO REAL solution, pH 9). Blocking was performed (1 hour) in a solution of 1× tris-buffered saline supplemented with 0.5% Triton X-100 and 3% donkey serum, and tissue sections were incubated overnight at 4°C with mouse monoclonal antibodies MF-20 (1:2 dilution; Developmental Studies Hybridoma Bank at the University of Iowa) and fibronectin (1:250 dilution; L0791, Sigma) or with rabbit polyclonal antibodies against troponin-I (1:25 dilution; sc15768, Santa Cruz Biotechnology), collagen II (1:250 dilution; Ab34712, Abcam), collagen IV (1:250 dilution; Ab6586, Abcam), Ki67 (1:25 dilution; RM91-06-S, Thermo Fisher Scientific), or laminin (1:100 dilution; L9393, Sigma) or with rat polyclonal antibody against BrdU (1:25 dilution; OBT0030, Accurate Chemical and Scientific Co.). This was followed by incubation with the corresponding Alexa Fluor–conjugated secondary antibodies (1:200 dilution; Molecular Probes) for 2 hours at 37°C. Sections were then stained with DAPI (Invitrogen), mounted, examined, and photographed using a Leica TCS SP5 AOBS spectral confocal microscope.

In vivo BrdU pulse-chase labeling experiments

Apically resected ($n = 5$) and sham-operated ($n = 3$) neonatal mice were injected subcutaneously with 50 µl of a solution of BrdU (20 mg/ml; Roche Applied Science) at different days after surgery (see figs. S1E and S2E). The hearts were then harvested at different time points following surgery and processed histologically as described above. For each heart, we averaged the number of $Tnni3^+/BrdU^+$ or $MF\text{-}20^+/BrdU^+$ cells across four fields of view randomly chosen around the injured area (border zone) or at a distant area within the left ventricle (remote zone) for four different planes of section across the entire injured area of the apex. To assess CM proliferation in experiments involving P1 neonates, a 100-µm × 100-µm grid (10,000 μm^2) was laid over images, taken at ×63 magnification, of each amputated or sham-operated heart, analyzing an average of four different planes of sections within the apex of each heart, and the number of $BrdU^+/Tnni3^+$ cells within that area was counted. To count proliferating CMs in experiments involving P2 neonates, the number of $MF\text{-}20^+/BrdU^+$ cells was calculated in consecutive images, taken at ×40 magnification, spanning a total area of 0.1 mm^2. For both P1 and P2 hearts, only fields completely filled with cells were included in the analysis. DAPI was used to counterstain nuclei and helped to distinguish mono- and binucleated CMs. Representative images were taken at ×63 magnification for P1 hearts and at ×40 magnification for P2 hearts.

Treatment with BAPN and heart decellularization

For BAPN treatment, we designed a protocol based on previously reported regimes of oral administration in adult (*44*) and neonatal (*34*) mice. In brief, pregnant 6- to 10-week-old female CD1 mice were treated with BAPN (1 mg/ml; in drinking water) for 17 days, beginning on the fifth dpc and ending on the third day post-partum. The volume of drinking water consumed was monitored weekly to assess the average dose of BAPN ingested by the mice, which amounted to ~5 mg of BAPN per mouse per day (~125 mg/kg per day). For decellularization experiments, hearts were harvested without great vessels and atria, quickly placed in warm (37°C) PBS to allow the blood to leave the ventricle chamber, snap-frozen using liquid N_2, and stored at −80°C until use. Hearts underwent three cycles of freeze/thawing to damage the cellular membrane. To keep a similar size and weight of the myocardial tissue to be decellularized in between different mouse ages, a similar slice in weight of myocardial tissue was cut for all the hearts analyzed. Myocardial organs were decellularized in autoclaved 2-ml Eppendorf tube in the orbital shaker (GyroMini) with decellularized buffers (0.2% Triton X-100, 0.4% Triton X-100 in PBS, and 25 mM EDTA) for 24 hours. After decellularization, hearts were washed using PBS and finally water. We then cryosectioned and analyzed the structure by immunofluorescence analysis, by various colorimetric techniques, or by AFM.

Atomic force microscopy

Mechanical measurements were carried out with a custom-built atomic force microscope (TE2000, Nikon). Measurements were performed at room temperature with four-slide pyramidal tips attached to cantilevers with a nominal spring constant (k) of 0.03 N/m (MLCT, Bruker). To compute the effective Young's modulus of the ECM, 10 force displacement curves (F-z) were recorded at 1 Hz with a peak-to-peak amplitude of 5 µm. In hearts, measurements were taken in three different regions of the ventricles, corresponding to pericardium, myocardium, and endocardium. The regions of interest for AFM measurements were identified by means of phase-contrast images recorded with the inverted

optical microscope. For each region of interest, AFM measurements were taken in five separated by 10 μm.

Quantitative real-time PCR

Total RNA was extracted from only the ventricles of different hearts at various days after apical resection surgery. Briefly, samples were treated in TRIzol reagent, and total RNA was extracted using the miRNA Easy Kit (Qiagen) following the manufacturer's instructions. For complementary DNA (cDNA) synthesis, 25 or 50 μg of total RNA was reverse-transcribed using the Cloned AMV First-Strand cDNA Synthesis Kit (Invitrogen), and all qRT-PCRs were performed in technical triplicates. Detection of different PCR products was monitored by measuring the increase in fluorescence caused by the binding of SYBR Green dye. All qRT-PCRs were run with an Applied Biosystems 7900 HT Fast qRT-PCR System thermocycler following the manufacturer's instructions. The qRT-PCR data were obtained by normalizing the raw data against two stably expressed endogenous control genes (*Gapdh* and *Rlp13*), as determined by the ΔC_t method.

RNA-seq and analysis

Total RNA was extracted from only the ventricles of P1 ($n = 3$) or P2 ($n = 3$) hearts using QIAzol lysis reagent (Qiagen) and RNeasy extraction kit (Qiagen) according to the manufacturer's instructions. Polyadenylated RNA was isolated from 1 to 5 μg of total RNA using the Dynabeads mRNA Purification Kit (Invitrogen). Polyadenylated RNA was then fragmented, retro-transcribed, and finally resynthesized to double-stranded DNA molecules using DNA polymerase I (Invitrogen). End-pair, A-tailing, adapter ligation, and size selection were then performed. RNA-seq analysis was performed using the 50-nucleotide-long paired-end reads obtained from sequencing six samples of mouse heart tissue at two different time points and using three biological replicates for each time point. First, the quality of the reads was verified using FastQC v0.11.21. Then, the reads were mapped to *Mus musculus* reference genome vGRCm38 2, using TopHat v2.0.143. Following mapping, the transcript and normalization counts were performed using Cuffdiff v2.2.1 4. The differential expression analysis of normalized counts was performed using cummeRbund v2.12 5, a widely used R v3.2 package that works together with the Cuffdiff software; the applied threshold on the parameter α in the function getSig of the package was ≤0.05. Last, the differentially expressed genes were visualized using the heat map.

Statistical analysis

All data obtained from various experiments followed a normal distribution and were analyzed using an unpaired two-tailed *t* test. All data are means ± SEM. Statistical analyses were carried out using the GraphPad Prism software.

SUPPLEMENTARY MATERIALS

Supplementary material for this article is available at http://advances.sciencemag.org/cgi/content/full/4/5/eaao5553/DC1

fig. S1. Procedure for resection of the left ventricular apex in neonatal mice and long-term effects of amputation surgery in P1 and older mice.

fig. S2. Scar and new myocardial tissue assessment following surgical amputation of the left ventricular apex in P2 mice revealed a lack of myocardial regeneration.

fig. S3. Lack of regeneration following amputation of the left ventricular apex in P3 and P4 mice.

fig. S4. Lack of regeneration following amputation of the left ventricular apex in P9 mice.

fig. S5. Differentially expressed genes in the ventricles of hearts from P1 and P2 mice.

fig. S6. Expression level of ECM proteins in P1 and P2 and relative size of resected tissue in BAPN-related experiments.

Supplementary Dataset. List of transcripts differentially expressed in P1 and P2 neonatal mouse hearts.

REFERENCES AND NOTES

1. B. B. Kelly, J. Narula, V. Fuster, Recognizing global burden of cardiovascular disease and related chronic diseases. *Mt. Sinai J. Med.* **79**, 632–640 (2012).
2. A. P. Beltrami, K. Urbanek, J. Kajstura, S.-M. Yan, N. Finato, R. Bussani, B. Nadal-Ginard, F. Silvestri, A. Leri, C. A. Beltrami, P. Anversa, Evidence that human cardiac myocytes divide after myocardial infarction. *N. Engl. J. Med.* **344**, 1750–1757 (2001).
3. L. H. Opie, P. J. Commerford, B. J. Gersh, M. A. Pfeffer, Controversies in ventricular remodelling. *Lancet* **367**, 356–367 (2006).
4. K. D. Poss, L. G. Wilson, M. T. Keating, Heart regeneration in zebrafish. *Science* **298**, 2188–2190 (2002).
5. A. Raya, C. M. Koth, D. Büscher, Y. Kawakami, T. Itoh, R. M. Raya, G. Sternik, H.-J. Tsai, C. Rodriguez-Esteban, J. C. Izpisúa-Belmonte, Activation of Notch signaling pathway precedes heart regeneration in zebrafish. *Proc. Natl. Acad. Sci. U.S.A.* **100** (suppl. 1), 11889–11895 (2003).
6. Á. Raya, A. Consiglio, Y. Kawakami, C. Rodriguez-Esteban, J. C. Izpisúa-Belmonte, The zebrafish as a model of heart regeneration. *Cloning Stem Cells* **6**, 345–351 (2004).
7. C. Jopling, E. Sleep, M. Raya, M. Martí, A. Raya, J. C. Izpisúa Belmonte, Zebrafish heart regeneration occurs by cardiomyocyte dedifferentiation and proliferation. *Nature* **464**, 606–609 (2010).
8. K. Kikuchi, Advances in understanding the mechanism of zebrafish heart regeneration. *Stem Cell Res.* **13**, 542–555 (2014).
9. E. R. Porrello, A. I. Mahmoud, E. Simpson, J. A. Hill, J. A. Richardson, E. N. Olson, H. A. Sadek, Transient regenerative potential of the neonatal mouse heart. *Science* **331**, 1078–1080 (2011).
10. G. Tao, P. C. Kahr, Y. Morikawa, M. Zhang, M. Rahmani, T. R. Heallen, L. Li, Z. Sun, E. N. Olson, B. A. Amendt, J. F. Martin, Pitx2 promotes heart repair by activating the antioxidant response after cardiac injury. *Nature* **534**, 119–123 (2016).
11. Y. Morikawa, M. Zhang, T. Heallen, J. Leach, G. Tao, Y. Xiao, Y. Bai, W. Li, J. T. Willerson, J. F. Martin, Actin cytoskeletal remodeling with protrusion formation is essential for heart regeneration in Hippo-deficient mice. *Sci. Signal.* **8**, ra41 (2015).
12. C. Han, Y. Nie, H. Lian, R. Liu, F. He, H. Huang, S. Hu, Acute inflammation stimulates a regenerative response in the neonatal mouse heart. *Cell Res.* **25**, 1137–1151 (2015).
13. W. Yu, X. Huang, X. Tian, H. Zhang, L. He, Y. Wang, Y. Nie, S. Hu, Z. Lin, B. Zhou, W. Pu, K. O. Lui, B. Zhou, GATA4 regulates Fgf16 to promote heart repair after injury. *Development* **143**, 936–949 (2016).
14. Z. Chen, J. Xie, H. Hao, H. Lin, L. Wang, Y. Zhang, L. Chen, S. Cao, X. Huang, W. Liao, J. Bin, Y. Liao, Ablation of periostin inhibits post-infarction myocardial regeneration in neonatal mice mediated by the phosphatidylinositol 3 kinase/glycogen synthase kinase 3β/cyclin D1 signalling pathway. *Cardiovasc. Res.* **113**, 620–632 (2017).
15. E. Bassat, Y. E. Mutlak, A. Genzelinakh, I. Y. Shadrin, K. Baruch Umansky, O. Yifa, D. Kain, D. Rajchman, J. Leach, D. Riabov Bassat, Y. Udi, R. Sarig, I. Sagi, J. F. Martin, N. Bursac, S. Cohen, E. Tzahor, The extracellular matrix protein agrin promotes heart regeneration in mice. *Nature* **547**, 179–184 (2017).
16. Y. Morikawa, T. Heallen, J. Leach, Y. Xiao, J. F. Martin, Dystrophin–glycoprotein complex sequesters Yap to inhibit cardiomyocyte proliferation. *Nature* **547**, 227–231 (2017).
17. S. Ai, X. Yu, Y. Li, Y. Peng, C. Li, Y. Yue, G. Tao, C. Li, W. T. Pu, A. He, Divergent requirements for EZH1 in heart development versus regeneration. *Circ. Res.* **121**, 106–112 (2017).
18. S. A. Muralidhar, A. I. Mahmoud, D. Canseco, F. Xiao, H. A. Sadek, Harnessing the power of dividing cardiomyocytes. *Glob. Cardiol. Sci. Pract.* **2013**, 212–221 (2013).
19. M. H. Soonpaa, K. K. Kim, L. Pajak, M. Franklin, L. J. Field, Cardiomyocyte DNA synthesis and binucleation during murine development. *Am. J. Physiol.* **271**, H2183–H2189 (1996).
20. E. R. Porrello, B. A. Johnson, A. B. Aurora, E. Simpson, Y. J. Nam, S. J. Matkovich, G. W. Dorn II, E. van Rooij, E. N. Olson, MiR-15 family regulates postnatal mitotic arrest of cardiomyocytes. *Circ. Res.* **109**, 670–679 (2011).
21. D. C. Andersen, S. Ganesalingam, C. H. Jensen, S. P. Sheikh, Do neonatal mouse hearts regenerate following heart apex resection? *Stem Cell Reports* **2**, 406–413 (2014).
22. D. M. Bryant, C. C. O'Meara, N. N. Ho, J. Gannon, L. Cai, R. T. Lee, A systematic analysis of neonatal mouse heart regeneration after apical resection. *J. Mol. Cell. Cardiol.* **79**, 315–318 (2015).
23. T. Konfino, N. Landa, T. Ben-Mordechai, J. Leor, The type of injury dictates the mode of repair in neonatal and adult heart. *J. Am. Heart Assoc.* **4**, e001320 (2015).
24. B. J. Haubner, M. Adamowicz-Brice, S. Khadayate, V. Tiefenthaler, B. Metzler, T. Aitman, J. M. Penninger, Complete cardiac regeneration in a mouse model of myocardial infarction. *Aging* **4**, 966–977 (2012).
25. Y. Nakada, W. Kimura, H. A. Sadek, Defining the limit of embryonic heart regeneration. *Circulation* **132**, 77–78 (2015).

26. M. Notari, J. Pulecio, Á. Raya, Update on the pathogenic implications and clinical potential of microRNAs in cardiac disease. *Biomed. Res. Int.* **2015**, 105620 (2015).
27. A. I. Mahmoud, F. Kocabas, S. A. Muralidhar, W. Kimura, A. S. Koura, S. Thet, E. R. Porrello, H. A. Sadek, Meis1 regulates postnatal cardiomyocyte cell cycle arrest. *Nature* **497**, 249–253 (2013).
28. B. D. Polizzotti, B. Ganapathy, S. Walsh, S. Choudhury, N. Ammanamanchi, D. G. Bennett, C. G. dos Remedios, B. J. Haubner, J. M. Penninger, B. Kühn, Neuregulin stimulation of cardiomyocyte regeneration in mice and human myocardium reveals a therapeutic window. *Sci. Transl. Med.* **7**, 281ra245 (2015).
29. A. I. Mahmoud, E. R. Porrello, W. Kimura, E. N. Olson, H. A. Sadek, Surgical models for cardiac regeneration in neonatal mice. *Nat. Protoc.* **9**, 305–311 (2014).
30. H. K. Gaggin, J. L. Januzzi Jr., Biomarkers and diagnostics in heart failure. *Biochim. Biophys. Acta* **1832**, 2442–2450 (2013).
31. M. J. Foglia, K. D. Poss, Building and re-building the heart by cardiomyocyte proliferation. *Development* **143**, 729–740 (2016).
32. E. Vuorio, B. de Crombrugghe, The family of collagen genes. *Annu. Rev. Biochem.* **59**, 837–872 (1990).
33. E. H. Tchaparian, J. Y. Uriu-Adams, C. L. Keen, A. E. Mitchell, R. B. Rucker, Lysyl oxidase and P-ATPase-7A expression during embryonic development in the rat. *Arch. Biochem. Biophys.* **379**, 71–77 (2000).
34. T. Mammoto, E. Jiang, A. Jiang, A. Mammoto, Extracellular matrix structure and tissue stiffness control postnatal lung development through the lipoprotein receptor-related protein 5/Tie2 signaling system. *Am. J. Respir. Cell Mol. Biol.* **49**, 1009–1018 (2013).
35. D. C. Andersen, C. H. Jensen, C. Baun, S. Hvidsten, D. C. Zebrowski, F. B. Engel, S. P. Sheikh, Persistent scarring and dilated cardiomyopathy suggest incomplete regeneration of the apex resected neonatal mouse myocardium—A 180 days follow up study. *J. Mol. Cell. Cardiol.* **90**, 47–52 (2016).
36. F. Li, X. Wang, J. M. Capasso, A. M. Gerdes, Rapid transition of cardiac myocytes from hyperplasia to hypertrophy during postnatal development. *J. Mol. Cell. Cardiol.* **28**, 1737–1746 (1996).
37. S. Walsh, A. Pontén, B. K. Fleischmann, S. Jovinge, Cardiomyocyte cell cycle control and growth estimation in vivo—An analysis based on cardiomyocyte nuclei. *Cardiovasc. Res.* **86**, 365–373 (2010).
38. A. F. Bayomy, M. Bauer, Y. Qiu, R. Liao, Regeneration in heart disease—Is ECM the key? *Life Sci.* **91**, 823–827 (2012).
39. J. G. Jacot, J. C. Martin, D. L. Hunt, Mechanobiology of cardiomyocyte development. *J. Biomech.* **43**, 93–98 (2010).
40. R. O. Hynes, The extracellular matrix: Not just pretty fibrils. *Science* **326**, 1216–1219 (2009).
41. F. Guilak, D. M. Cohen, B. T. Estes, J. M. Gimble, W. Liedtke, C. S. Chen, Control of stem cell fate by physical interactions with the extracellular matrix. *Cell Stem Cell* **5**, 17–26 (2009).
42. N. L. Tulloch, V. Muskheli, M. V. Razumova, F. S. Korte, M. Regnier, K. D. Hauch, L. Pabon, H. Reinecke, C. E. Murry, Growth of engineered human myocardium with mechanical loading and vascular coculture. *Circ. Res.* **109**, 47–59 (2011).
43. Y. Yahalom-Ronen, D. Rajchman, R. Sarig, B. Geiger, E. Tzahor, Reduced matrix rigidity promotes neonatal cardiomyocyte dedifferentiation, proliferation and clonal expansion. *eLife* **4**, e07455 (2015).
44. A. Mammoto, T. Mammoto, M. Kanapathipillai, C. Wing Yung, E. Jiang, A. Jiang, K. Lofgren, E. P. S. Gee, D. E. Ingber, Control of lung vascular permeability and endotoxin-induced pulmonary oedema by changes in extracellular matrix mechanics. *Nat. Commun.* **4**, 1759 (2013).

Acknowledgments: We thank C. Morera and C. Pardo for technical assistance, as well as all members of Center of Regenerative Medicine in Barcelona (CMRB) for stimulating discussion on this study. We also thank B. J. Haubner for valuable help in setting up surgical procedures. **Funding:** M.N. and S.J.B.-G. were partially supported by the Spanish Ministry of Economy and Competitiveness (MINECO) through Ayuda para la Formación Posdoctoral (FPDI-2013-18459) and the Ramón y Cajal program (RYC-2012-10053), respectively. Additional funding for this project came from Generalitat de Catalunya (2017-SGR-899 and PERIS SLT002/16/00234), MINECO (SAF2015-69706-R and PI14-00280), ISCIII/FEDER (RD16/0011/0024), Fundació La Marató de TV3 (201534-30), and CERCA Programme/Generalitat de Catalunya.
Author contributions: M.N. and Á.R. designed the research; M.N. and A.V.-R. performed the surgical procedure in neonatal mice; M.N., S.J.B.-G., I.J., and L.M. performed the research; M.N., M.M., D.N., and Á.R. analyzed the data; and M.N., S.J.B.-G., and Á.R. wrote the paper.
Competing interests: The authors declare that they have no competing interests. **Data and materials availability:** All data needed to evaluate the conclusions in the paper are present in the paper and/or the Supplementary Materials. The transcriptomic data discussed in this publication have been deposited in Gene Expression Omnibus (GEO) of the National Center for Biotechnology Information and are accessible through GEO Series accession number GSE109660 (www.ncbi.nlm.nih.gov/geo/query/acc.cgi?acc=GSE109660). Additional data related to this paper may be requested from the authors.

Submitted 2 August 2017
Accepted 20 March 2018
Published 2 May 2018
10.1126/sciadv.aao5553

Citation: M. Notari, A. Ventura-Rubio, S. J. Bedford-Guaus, I. Jorba, L. Mulero, D. Navajas, M. Martí, Á. Raya, The local microenvironment limits the regenerative potential of the mouse neonatal heart. *Sci. Adv.* **4**, eaao5553 (2018).